ACSNANO
www.acsnano.org
ARTICLE

Three-Dimensional Optical Mapping of Nanoparticle Distribution in Intact Tissues

Shrey Sindhwani,[†,¶] Abdullah Muhammad Syed,[†,¶] Stefan Wilhelm,[†] Dylan R. Glancy,[‡] Yih Yang Chen,[†] Michael Dobosz,[§] and Warren C. W. Chan*[,†,‡,∥,⊥,#]

[†]Institute of Biomaterials and Biomedical Engineering, University of Toronto, Rosebrugh Building, Room 407, 164 College Street, Toronto, Ontario M5S 3G9, Canada

[‡]Department of Chemistry, University of Toronto, 80 St. George Street, Toronto, Ontario M5S 3H6, Canada

[§]Discovery Oncology, Pharmaceutical Research and Early Development, Roche Innovation Center Munich, Nonnenwald 2, 82377 Penzberg, Germany

[∥]Terrence Donnelly Centre for Cellular and Biomolecular Research, University of Toronto, 160 College Street, Room 230, Toronto, Ontario M5S 3E1, Canada

[⊥]Department of Chemical Engineering, University of Toronto, 200 College Street, Toronto, Ontario M5S 3E5, Canada

[#]Department of Material Science and Engineering, University of Toronto, 184 College Street, Suite 140, Toronto, Ontario M5S 3E1, Canada

Supporting Information

ABSTRACT: **The role of tissue architecture in mediating nanoparticle transport, targeting, and biological effects is unknown due to the lack of tools for imaging nanomaterials in whole organs. Here, we developed a rapid optical mapping technique to image nanomaterials in intact organs *ex vivo* and in three-dimensions (3D). We engineered a high-throughput electrophoretic flow device to simultaneously transform up to 48 tissues into optically transparent structures, allowing subcellular imaging of nanomaterials more than 1 mm deep into tissues which is 25-fold greater than current techniques. A key finding is that nanomaterials can be retained in the processed tissue by chemical cross-linking of surface adsorbed serum proteins to the tissue matrix, which enables nanomaterials to be imaged with respect to cells, blood vessels, and other structures. We developed a computational algorithm to analyze and quantitatively map nanomaterial distribution. This method can be universally applied to visualize the distribution and interactions of materials in whole tissues and animals including such applications as the imaging of nanomaterials, tissue engineered constructs, and biosensors within their intact biological environment.**

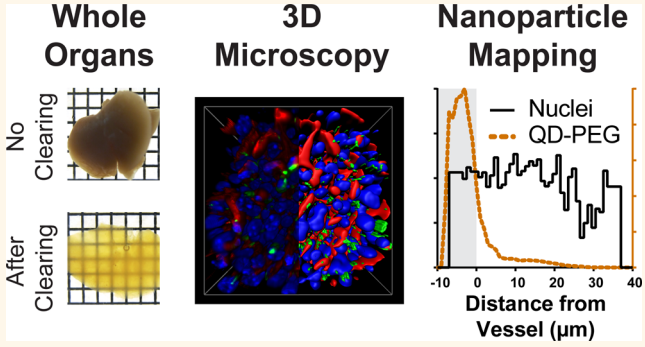

KEYWORDS: *3D imaging, microscopy, nanoparticles, optical clearing, CLARITY, nanoparticle biological interactions, whole organ distribution, nanotoxicology, nano−bio interface, nanosystems, protein corona*

Nanoparticles can be designed to target individual cell types in living organisms if they can overcome biological barriers to transport.[1−4] These barriers are poorly characterized due to a lack of tools for capturing the three-dimensional (3D) distribution of nanoparticles with respect to biological structures at subcellular resolution.[5−8] Current techniques can quantify the total nanoparticle accumulation in organs using elemental analysis (ICP-MS, inductively coupled plasma−mass spectrometry) and provide its gross anatomical distribution using MRI (magnetic resonance imaging), CT (X-ray computed tomography), Ultrasound, PET (positron emission tomography), whole animal fluorescence or radiolabeling. However, these systems level techniques cannot resolve the interactions of nanoparticles with respect to the cells, blood vessels and other structural components of tissues which mediate the biological response to nanomaterials. To achieve this resolution, researchers use flow cytometry and immunohistochemistry to examine nanoparticle distribution at the cellular level, but these techniques destroy the 3D architecture of the tissues that are analyzed. Currently, no technique is able to bridge

Received: March 17, 2016
Accepted: April 21, 2016
Published: April 21, 2016

DOI: 10.1021/acsnano.6b01879
ACS Nano 2016, 10, 5468−5478

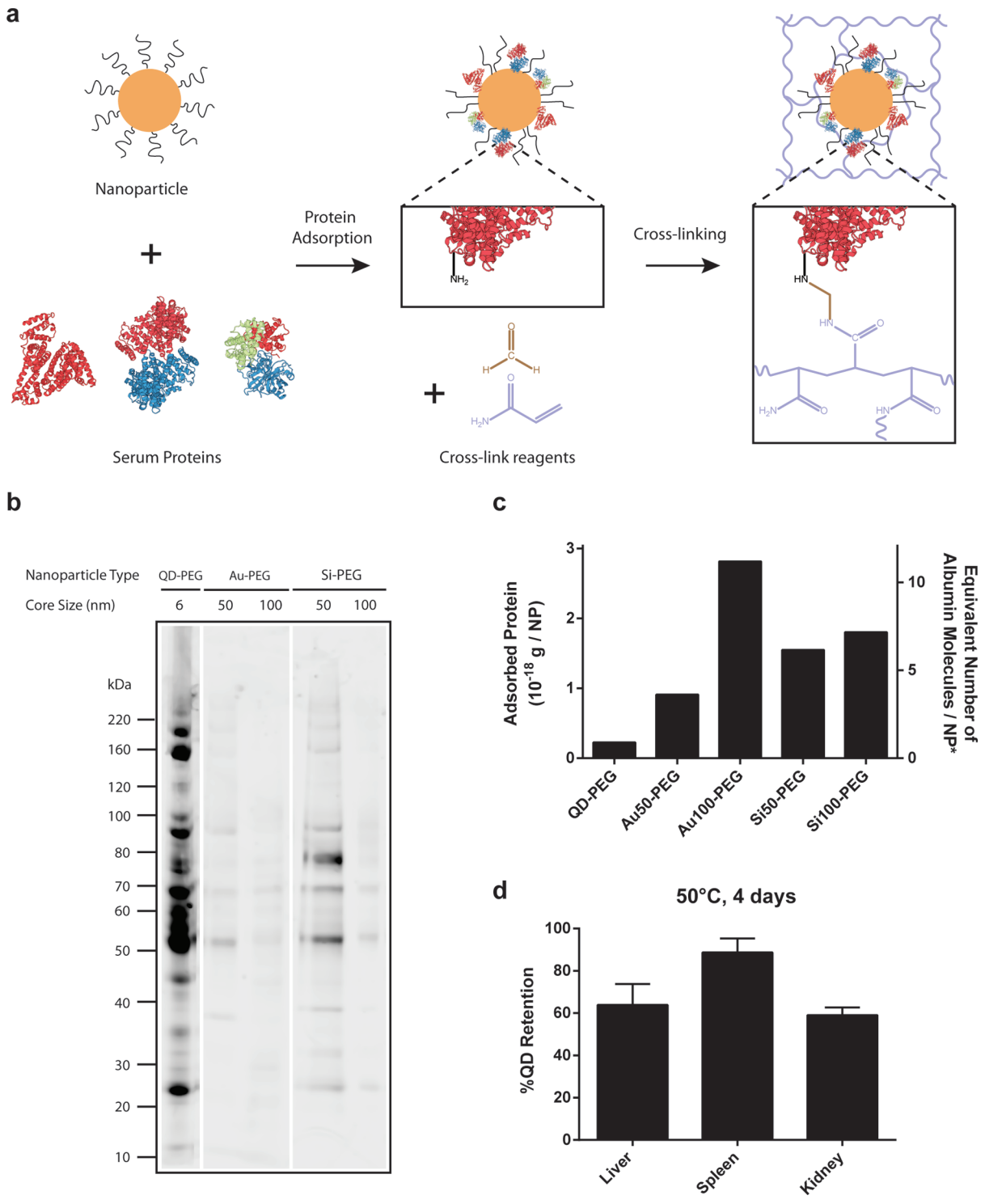

Figure 1. Nanoparticles are retained in tissues through the cross-linking of surface bound serum proteins. (a) Nanoparticles exposed to serum are quickly coated with a layer of serum proteins. These proteins can then be cross-linked into tissue using any available amine groups such as those found at the N-terminus or in lysine residues. Cross-linking of these proteins traps nanoparticles within tissue. (b) SDS-PAGE shows that a large variety of proteins adsorb to the nanoparticle surface irrespective of nanoparticle size or composition and even in the presence of polyethylene glycol (PEG) antifouling coating. (c) On a per nanoparticle basis, larger nanoparticles have more proteins on their surface which improves the efficiency of this cross-linking method. (d) After clearing at 50 °C for 4 days, QD-PEGs, the smallest nanoparticles in this group, are retained up to 95% (n = 3) in spleen tissues and ~70% overall in the tissue types relevant to nanoparticle accumulation and clearance. Error bars show standard deviation. QD-PEG, quantum dot with polyethylene glycol. Au-PEG, gold nanoparticle with polyethylene glycol. Si-PEG, silica nanoparticle with polyethylene glycol. * adsorbed protein divided by molecular mass of albumin (2×10^{-19} g).

this gap and visualize nanoparticles with subcellular resolution over whole organs. This is important because the 3D architecture of organs including the arrangement of blood vessels, lymphatics, and distribution of cells forms the major barriers to nanoparticle transport. Here, we developed a high-throughput technique that enables the quantitative 3D optical imaging of nanomaterials

DOI: 10.1021/acsnano.6b01879
ACS Nano 2016, 10, 5468−5478

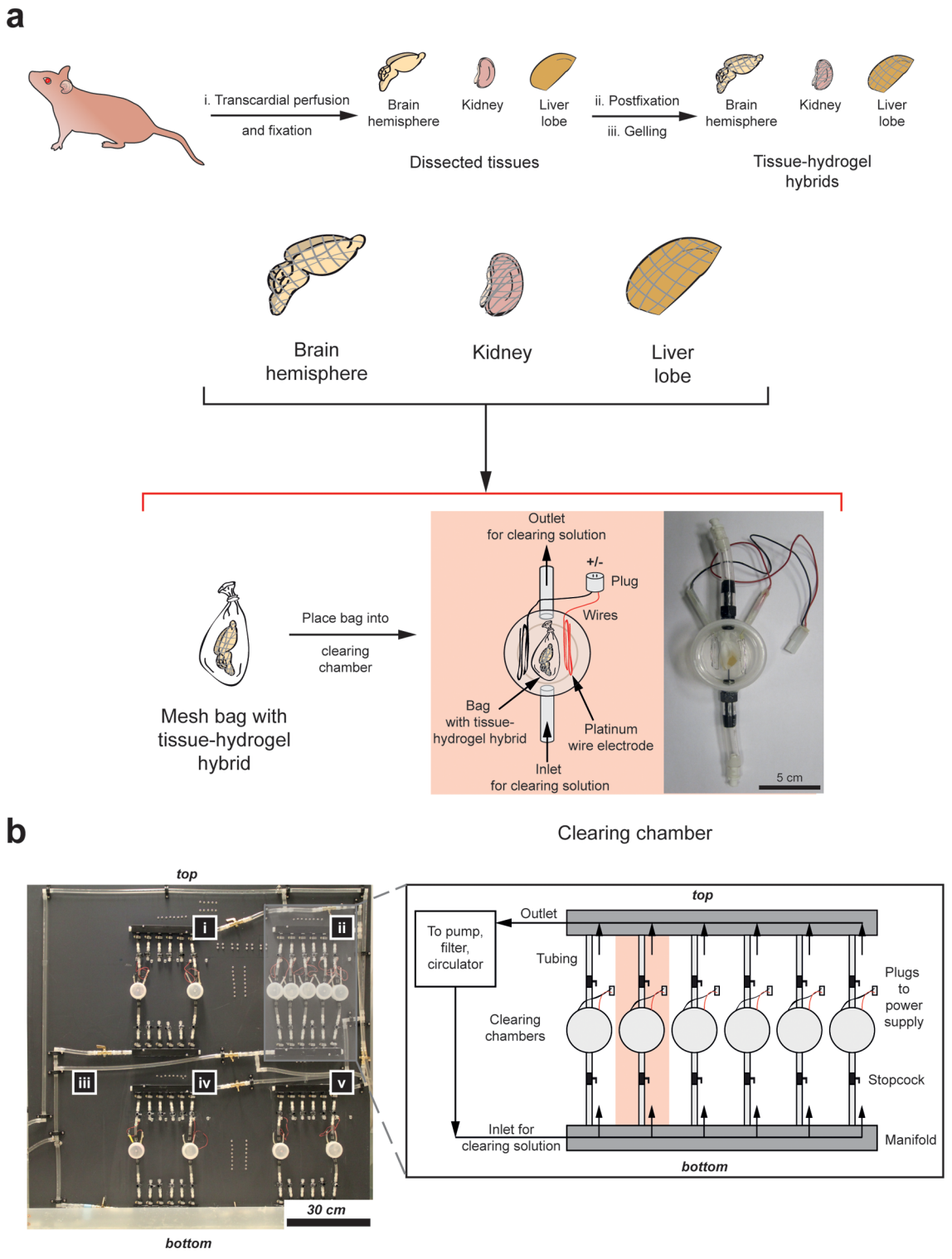

Figure 2. High-throughput clearing device and process flow. (a) QD-PEG were injected *via* tail vein into CD1 Nude mice. After transcardial perfusion and fixation, gelled whole or partial tissue−hydrogel hybrids were cleared using electrophoresis. Tissues were enclosed in mesh bags for protection and placed in a chamber between platinum electrodes. Chambers were then added to the high-throughput device vertically. (b) Photograph of a high-throughput clearing system. Clearing chambers were arrayed in clusters containing 6 chambers each. Four clusters (i, ii, iv, v) were constructed on one side of a PVC board, which allowed parallel clearing with up to 4 circulators running at different conditions (temperature, voltage, clearing solutions) simultaneously. This high-throughput system is modular and scalable with the potential for adding more clusters (iii). Pump, filters, circulator and electronic power supply not shown (they are behind board). Flow rate of 3−8 L/min was achieved using two centrifugal pumps in series with negative pressure to reduce risk of leakage.

in murine organs. The throughput of this technique is critical to its broad utility because it allows researchers to clear a larger number of samples which improves the statistical power of the experiments.

DOI: 10.1021/acsnano.6b01879
ACS Nano 2016, 10, 5468−5478

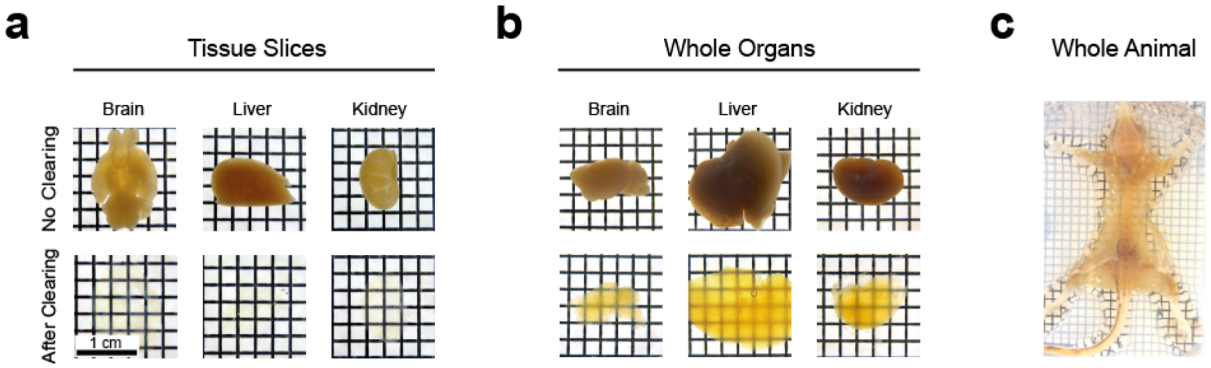

Figure 3. Clearing can be applied to tissues at any size scale. (a) One millimeter tissue slices and (b) intact organs from mice injected with nanomaterials become transparent after clearing and refractive index matching. (c) Nanomaterial distribution can also be visualized in whole animals after clearing through cardiac perfusion.

RESULTS AND DISCUSSION

To optically image nanoparticles and structural features in whole organs, these organs need to be transparent.[9−11] We based our approach for rendering tissues transparent on a previously developed technique by Chung *et al.* (CLARITY).[9] The first step is to chemically cross-link the entire tissue with an acrylamide hydrogel. This reaction cross-links primary amines on the N-terminus and the side chains of lysine residues to the acrylamide monomer to produce an acyl−urea bond (see Figure 1a). The tissue is then incubated with the surfactant sodium dodecyl sulfate (SDS), which emulsifies and removes lipids as they do not cross-link into the tissue due to the lack of amine groups. The removal of lipids is important because their presence in membranes is responsible for the majority of light scattering in tissues. The clearing process can be further accelerated by using electrophoresis (25 V, 37°C) to increase the mobility of charged SDS micelles across the tissue. As a result, the tissue becomes clear and allows light to penetrate in and out of the tissue. This approach preserves biological structures, renders tissues transparent, and can be used in conjunction with optical microscopy to create 3D representations of the tissue architecture. The remaining challenges in this approach are to determine whether nanoparticles can be retained and visualized and to increase the scale and flexibility of the tissue clearing process.

To visualize nanomaterials in whole organs, they have to be retained during the clearing process. Unlike proteins, nanoparticles are typically synthesized and coated with surface ligands such as polyethylene glycol (PEGs). The nanoparticle surface chemistry and therefore the chemical functional groups on their surface can be diverse depending on the biological and medical applications for which they are designed.[12] This means that the chemistry of the nanoparticle itself cannot be exploited to preserve nanoparticles within the tissue during the clearing process. When nanoparticles are injected into the bloodstream, proteins from serum adsorb on to the nanoparticle surface and this process has been observed for all types of nanoparticles studied so far.[4,13] We hypothesized that these proteins would be cross-linked into tissue around the nanoparticles thereby trapping them inside (Figure 1a).

We first determined the effect of serum proteins on nanoparticle−tissue retention during clearing. We examined this using nanoparticles coated with methoxy-terminated PEG, which is an antifouling chemical coating reported to have low serum protein adsorption.[14] Importantly, this PEG has no amine functional groups and thus cannot be chemically cross-linked into tissue directly. We rationalized that, if nanoparticles are cross-linked into tissue despite this coating, then other materials with alternative surface coatings would also be readily cross-linked within the tissue matrix. PEG coated ZnS capped CdSe quantum dots (QD-PEG; ∼6 nm core diameter, emission peak of 590 nm), gold nanoparticles (Au-PEG; 50 and 100 nm core diameters) and silica nanoparticles (Si-PEG; 50 and 100 nm core diameters) were incubated with 100% mouse serum for 24 h at 37°C. Protein characterization and total protein adsorption was measured using SDS-PAGE and BCA, respectively (Figure 1b,c). Initially, we evaluated the serum protein adsorption onto QD-PEG surfaces. Our results showed that 0.35 $\mu g/cm^2$ of proteins bound to their surface which corresponds to 2×10^{-19} g of protein per nanoparticle (Figure 1c). This mass of protein is approximately equivalent to a single albumin molecule (molecular weight, MW 70 kDa) bound to each QD-PEG. A single albumin molecule contains 51 lysine residues, each containing a reactive amine group, so this level of protein adsorption should be sufficient for cross-linking QD to the tissue matrix (Figure 1c). For Au-PEG and Si-PEG, the total quantity of adsorbed protein was equivalent to 4−12 albumin molecules. This increase in protein adsorption should further increase the nanoparticle cross-linking efficiency to tissues (Figure 1c). We further used SDS-PAGE to show the diversity of serum proteins (range in MW of 10−220 kDa) adsorbed to the QD surface (Figure 1b).

Encouraged by these results, we then tested whether these surface proteins would allow nanoparticles to be retained in an organ after clearing. We injected 400 pmol of QD-PEG (physiochemical properties of the QDs are described in Figure S1) intravenously into CD1 Nude mice *via* tail vein. After 72 h of circulation, we sacrificed the mice by transcardial perfusion with 60 mL of PBS buffer followed by 80 mL of 2% acrylamide containing fixative solution (see detailed procedure in Methods). We collected various organs from each of the mice, postfixed for 7 days, and subsequently gelled the organs to form tissue−hydrogel hybrids. To quantify the retention of nanoparticles after clearing, we then digested both cleared and uncleared (positive controls) organs and quantified the amount of cadmium(II) ions using ICP-MS.[15] On average, 71 ± 18% of QDs were retained overall for liver, spleen, and kidney (2% acrylamide, 4% SDS clearing solution, 50 °C, and 25 V, see Figure 1d). These values represent the lower bound of nanoparticle retention because QDs are particularly small and have a relatively small amount of proteins per particle (Figure 1c). Using 50 and 100 nm Au-PEG, we observed 84 ± 23% and 122 ± 22% retention, respectively (Figure S2).

DOI: 10.1021/acsnano.6b01879
ACS Nano 2016, 10, 5468−5478

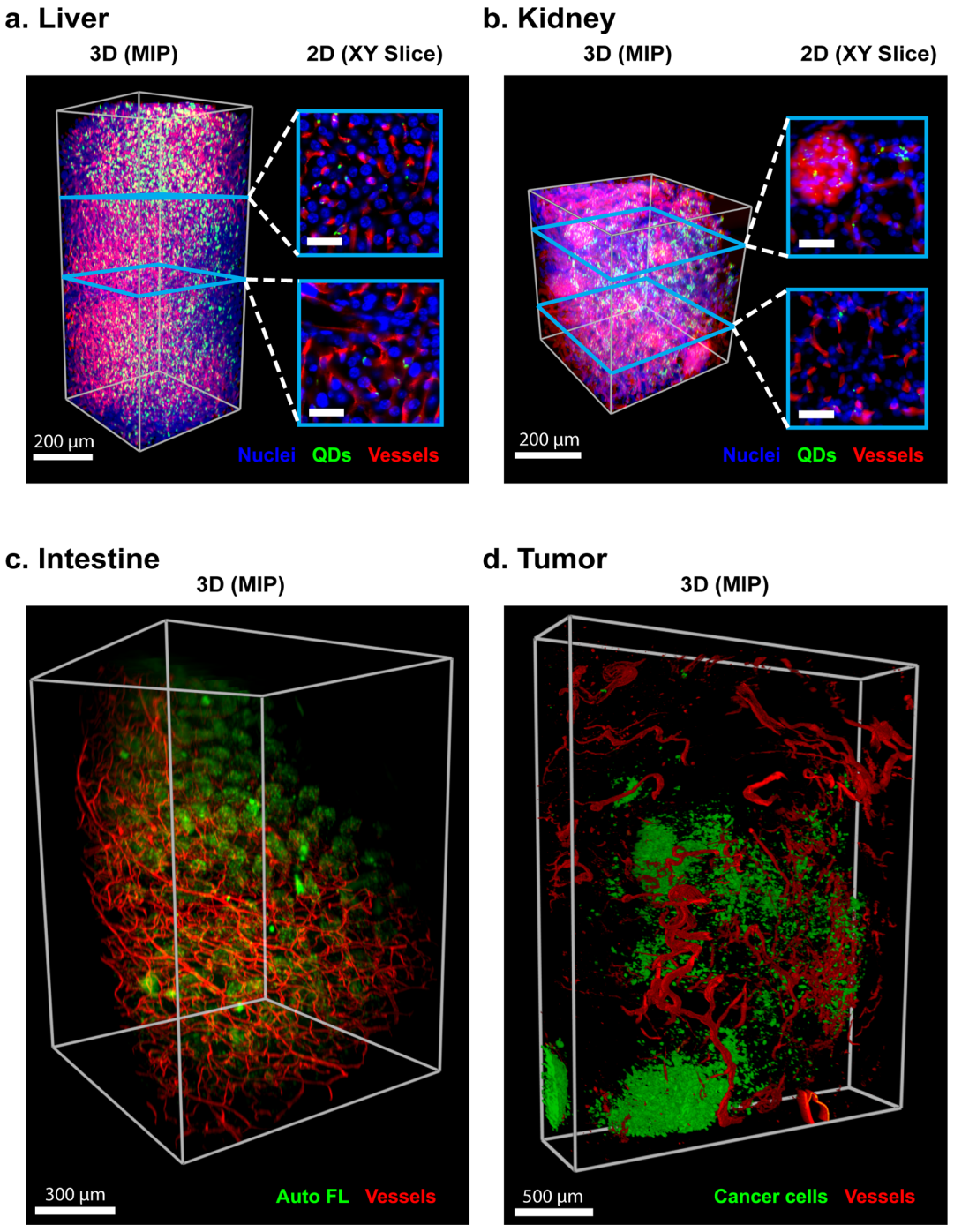

Figure 4. QD-PEG visualized in multiple organs. (a) 3D maximum intensity projection (MIP) and 2D *XY* projection of an image of cleared liver with nuclei labeled in blue (DAPI), blood vessels in red (GSL1-A647), and QD-PEG labeled in green. The corresponding 2D *XY* projection shows that most QD-PEG associate with blood vessels in apparent endosomal compartments. (b) 3D MIP and 2D *XY* projection of kidney show QD-PEG associated with vessels particularly in the glomeruli but absent from renal tubules. (c) 3D MIP of intestine (autofluorescence; Auto FL) and associated blood vessels (GSL1-A647). (d) 3D α-blend projection of tumor with MDA-MB-231 breast cancer cells expressing tdTomato and associated blood vessels (GSL1-A647), revealing the inherent heterogeneity of cancer tissue. Scale bars indicate 50 μm for 2D *XY* projections in (a) and (b). Original image was taken with voxel sizes of (a and b) 0.228 μm × 0.228 μm × 2.00 μm, (c) 0.572 μm × 0.572 μm × 2.00 μm, and (d) 1.24 μm × 1.24 μm × 7.3 μm. Liver images were obtained from 1 mm parasagittal sections. Kidney images were obtained using 1 mm coronal sections.

Once we determined that nanoparticles are retained in tissues, we then developed a clearing system that can process multiple organs simultaneously. Currently, tissue clearing is achieved using a single chamber design, but this approach is not suitable for analyzing the behavior of nanoparticles in tissues due to low throughput.[9] Typically, it takes approximately 30 days to clear tissues using an expensive commercial apparatus setup with conventional parameters. This means that a typical multifactorial study involving 100 organs would be either cost prohibitive if many clearing setups were purchased or time prohibitive because it would take more than 8 years to clear 100 organs. To address this problem, we developed a modular, high-throughput clearing

DOI: 10.1021/acsnano.6b01879
ACS Nano 2016, 10, 5468−5478

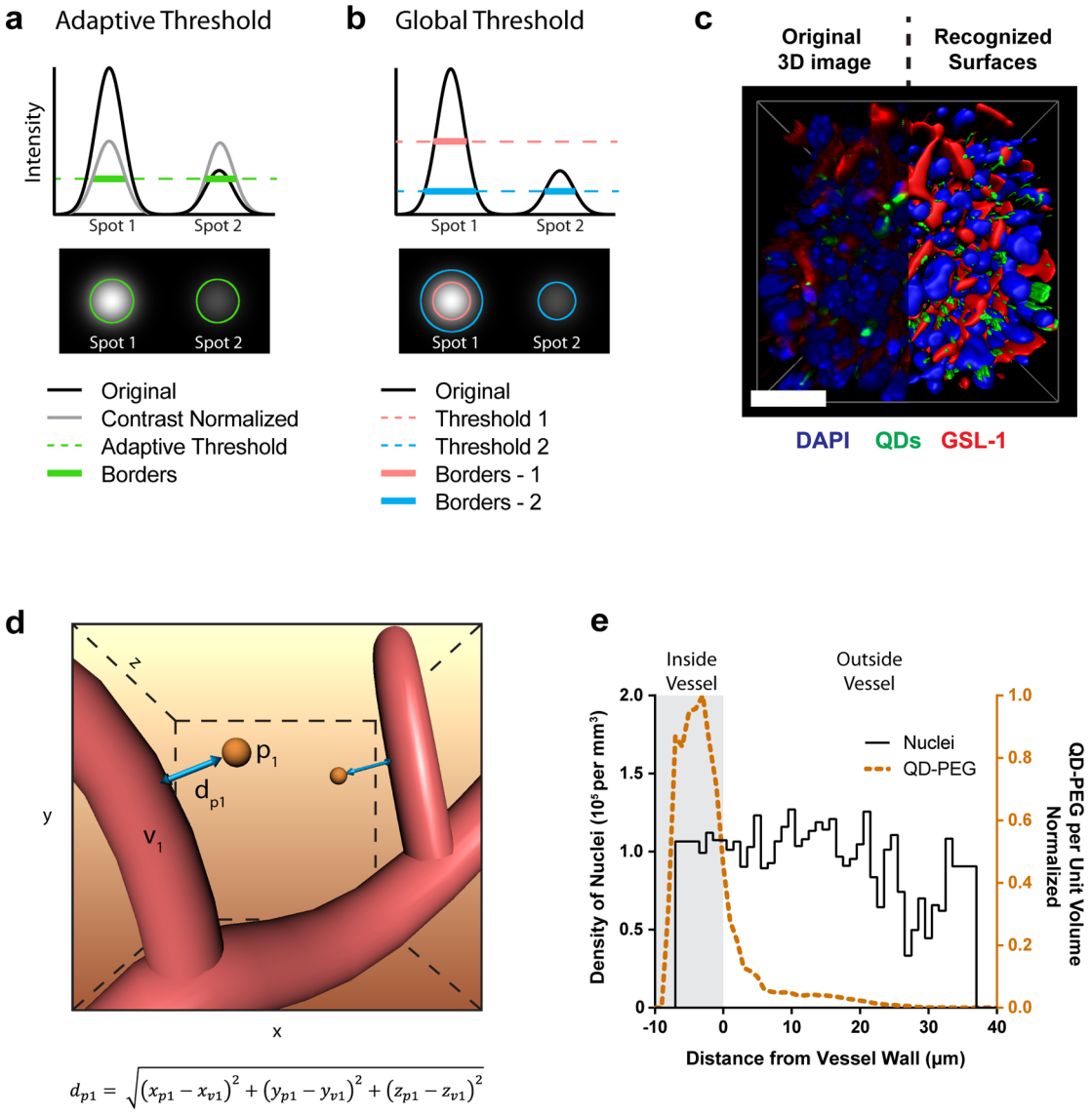

Figure 5. Image analysis scheme for examination of nanoparticle distribution. (a) Schematic showing how features can be detected using either an adaptive or a global threshold. Two Gaussian spots with equal size but varying intensity are shown as a line-plot above and 2D image below. The features were detected using an adaptive threshold in which the threshold depends on the average intensity of neighboring pixels. This is implemented here by creating a new image (contrast normalized) which is generated by dividing each pixel in the original image by the average of the 100 × 100 pixels in its neighborhood. A new threshold is applied to this image and is able to accurately estimate the full width at half-maximum of both spots. (b) Same as (a) but using two different global thresholds which are unable to accurately capture the full width at half-maximum of both spots. (c) Left: 3D α-blend projection of QD-PEG in liver with counterstaining for blood vessels and nuclei. Right: the recognized surfaces, calculated using a local threshold, around these features in the same image. Both sides are from the same original sample in order to visually demonstrate the transition from original image to recognized surfaces. (d) Schematic showing nanoparticles and their distances in 3D. The 3D distance is calculated using the formula shown for 3D Euclidean distance. (e) QD-PEG distribution and nuclei distribution with respect to distance from blood vessels. The average density of QD fluorescence outside blood vessels was only 7% of the density inside blood vessels, while the density of nuclei was constant with respect to the distance from the blood vessel. Scale bar shows 50 μm. Image captured using a voxel size of 0.228 μm × 0.228 μm × 2.00 μm.

device to process up to 48 tissues simultaneously. One distinct aspect of the device is that we engineered it with minimal components to reduce cost (Figure 2). We designed this device so that electrophoresis would simultaneously be conducted in 24 chambers, with flow evenly divided between these chambers. We ensured that each chamber could be plugged and unplugged independently from other chambers without any interruption or downtime in clearing in other parts of the device. For the analysis of different types of organs, it may be necessary to apply different conditions (*e.g.*, temperature, clearing solutions, and voltage). Therefore, we organized the chambers into four clusters. Each cluster had isolated tubing that can be connected to a different circulator if necessary. This multichamber system can clear a total of 48 tissues simultaneously if two tissues are used per chamber in 24 chambers (Figure 2b). This is possible because the internal volume per chamber is approximately 3 cm × 3 cm × 1 cm which is sufficient to accommodate approximately 2 whole mouse organs. The exact number of organs or tissues that can be used depends on the volume of the tissues so that 6 or more slices (1−2 mm thick) could easily be accommodated, but a whole liver

DOI: 10.1021/acsnano.6b01879
ACS Nano 2016, 10, 5468−5478

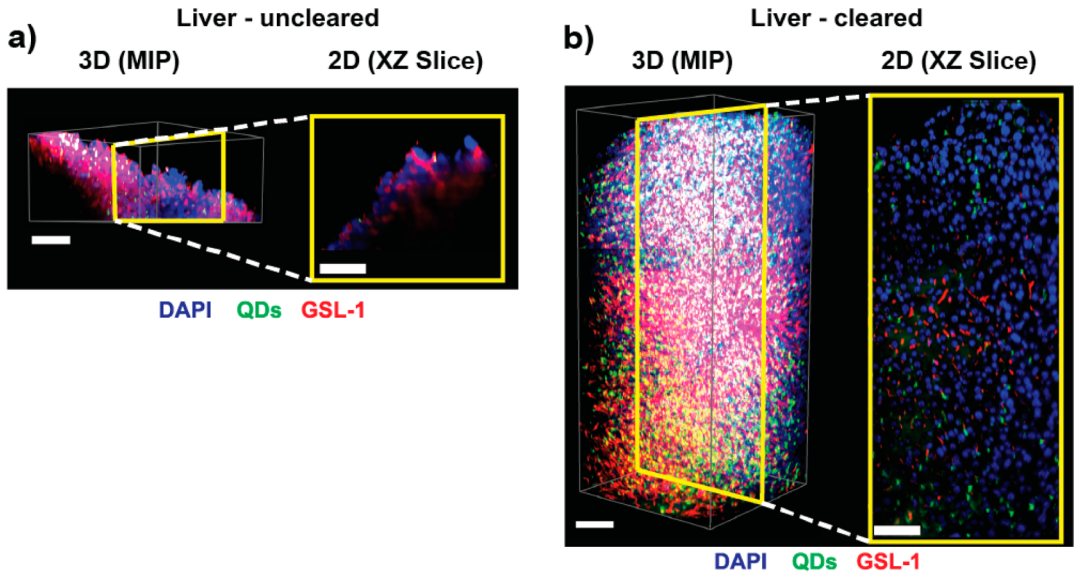

Figure 6. QD-PEG imaged up to 1 mm after processing. (a) 3D MIP and 2D *XZ* projections of an uncleared liver piece which can be imaged to a depth of ~40 μm or 3 cell layers before substantial blurring occurs. (b) 3D maximum intensity projection (MIP) and 2D *XZ* projection of an image of cleared liver with nuclei labeled in blue (DAPI), blood vessels in red (GSL1-A647), and QD-PEG labeled in green. No visible degradation in image quality is observed over 1000 μm of cleared liver. Scale bars indicate 100 μm.

from rats would be too large. We used this high-throughput system to screen and optimize clearing parameters (2% acrylamide, 4% SDS clearing solution, 50 °C, and 25 V) which further accelerated tissue clearing by 4.5-fold (Figure S3 and S4). After the clearing step, tissue slices and whole organs became transparent (Figure 3a,b). Alternatively, whole animals can be rendered transparent[16] potentially enabling the analysis of the entire biodistribution of nanoparticles with subcellular detail (Figure 3c). The combination of our enhanced protocol with the high-throughput clearing device can now enable 3D mapping of nanoparticle distribution in multiple organs with sufficient replicates to achieve statistically valid results.

With our enhanced clearing approach, we then examined the tissues involved in nanoparticle accumulation and clearance, using QD-PEG as the model nanoparticle. We cleared kidney, liver, and spleen tissues from animals injected with QD-PEG and successfully visualized quantum dot fluorescence in all three organ types (Figure 4, Figure S5 and Supporting Information Videos S1−S5). In the liver, the fluorescence of the QDs was confined to small and spherical compartments that are approximately 1 μm in diameter and lining the vasculature. These compartments are likely cell endosomes and/or lysosomes of either liver sinusoidal endothelial cells or Kupffer cells which are responsible for the uptake and processing of nanoparticles (Figure 4a, Supporting Information Videos S1 and S2).[17,18] We observed negligible uptake of QD-PEG in hepatocytes (recognizable in these images due to their large nuclei and prominent nucleoli). In the kidney, QD-PEG localized along the vasculature and in the renal corpuscle but not in the tubules, implying minimal renal clearance (Figure 4b, Supporting Information Videos S3 and S4). This is expected because the hydrodynamic size of QD-PEG was greater than the filtration cutoff of ~6 nm.[19−22] In the spleen, high tissue autofluorescence prevented the imaging of nuclei or vascular stains in most of the tissue (Figure S5c, Supporting Information Video S5). Despite this autofluorescence, QDs could still be visualized but their spatial context could not be interpreted. Other organs such as intestines (Figure 4c) and tumor (Figure 4d) can also be visualized using this technique. Overall, this enables the imaging of nanomaterials in whole tissues with subcellular resolution (Figure 4, Supporting Information Videos S1−S9), providing both a global perspective for visualizing long-range distribution patterns in organs and molecular level interactions between materials and biomolecules.

A next step was to quantitatively map the distribution of nanomaterials in whole tissues. We used biological features such as the vessels, nuclei, cells as reference points, which allowed us to numerically describe the location of the nanomaterials. In this process, we first created a new image where each voxel (unit of volume, analogous to pixel but in 3D) is labeled "1" at each location with a detected biological feature and "0" at all other locations. These features are detected by comparing the fluorescence intensity in each voxel to a threshold value. Since fluorescence signal from vessel staining varies over the length of a vessel, we used a local threshold normalized to the intensity of neighboring voxels over a 6 μm × 6 μm × 6 μm volume corresponding to the largest observed blood vessel (schematically illustrated in Figure 5, panel a *vs* b, which is a single threshold for the image). An example of the result of this process on a 3D image is shown in Figure 5c (right) where binary features corresponding to blood vessels, nuclei, and QD-PEG positive regions are shown beside the original image of these features (left). To identify the locations of the nuclei, we then use the mask on the nuclei channel and apply a 3D watershed algorithm to separate any merged nuclei. We then assign a unique identifier to each nuclei and determine the voxel closest to its center (the centroid) and calculate the minimum 3D Euclidean distance from this centroid and from each positive voxel on the QD-PEG mask to the nearest positive voxel on the blood vessel mask (Figure 5d). This analysis generates tables which list the fluorescence of QD-PEG and the number of nuclei at a given distance from the blood vessels. We applied this approach to a liver image with dimensions of 437 μm × 437 μm × 1000 μm and ~20 000 nuclei. Figure 5e shows a histogram of QD-PEG fluorescence density and the density of nuclei at a distance from a blood vessel. This histogram shows a clear trend of decaying

DOI: 10.1021/acsnano.6b01879
ACS Nano 2016, 10, 5468−5478

QD-PEG signal with respect to distance from the blood vessel wall. The average density of QD fluorescence outside blood vessels was only 7% of the density inside blood vessels, while the density of nuclei was constant with respect to the distance from blood vessels. Additionally, there are no QD-PEGs farther than 20 μm from the blood vessel. Using this method allows the quantitative comparison of the spatial distributions of nanomaterials within tissues.

Finally, we compare the improvement in imaging capability of cleared *versus* noncleared tissues. Currently, the cellular distribution of nanomaterials is most commonly analyzed using fluorescence microscopy on tissue slices which lose information about the 3D architecture of the tissue. Our technique overcomes this limitation through the transformation of tissues into transparent structures without the loss of nanomaterials. Using the liver as model tissue, we observed QD-PEGs up to 1 mm deep into tissue without any degradation in image quality in a cleared sample (Figure 6b), while there was substantial blurring and reduced signal intensity in uncleared tissue samples beyond 40 μm (Figure 6a). This represents a 25-fold improvement in the depth of imaging and therefore allows the distribution of nanoparticles to be mapped at subcellular resolution without losing information about the 3D architecture of the tissue.

CONCLUSION AND OUTLOOK

The ability to image deep into tissue is necessary in order to accurately reconstruct the 3D microstructure within whole organs. For example, in a tumor, nanoparticle transport is controlled by the structure of microvasculature, lymphatics, and the distribution of cells involved in nanoparticle uptake. This 3D, multiscale structure is destroyed by sectioning or digestion as necessitated by histopathology and flow cytometry. To address this problem, we achieved the analysis of nanoparticles in intact tissues at subcellular resolution by developing a high-throughput clearing device that can clear up to 48 tissues simultaneously and characterized the mechanism of nanoparticle retention within tissues during clearing. This approach enables us to image more than 1 mm deep into tissue and allows complex biological structures to be fully resolved. We envision that this approach can be used to elucidate the biological structures and barriers that govern nanoparticle transport in tumors and other organs which is necessary for targeting specific cell types *in vivo* (Supporting Information Videos S6–S9). In addition, our data on nanoparticle retention suggests that this technique can naturally be extended to luminescent nanoparticles such as carbon dots, carbon nanotubes, fullerenes, upconverting nanoparticles, and nanoparticles labeled with fluorescent tags such as gold and silica nanoparticles. Beyond nanotechnology applications, this technique can be universally applied to other areas of material science and engineering such as the analysis of tissue engineering constructs and implantable materials and biosensors.

METHODS

Quantum Dot Surface Modification with PEG and Characterization. The 590 nm emitting Alkyl Trilite CdSe quantum dots (solubilized in toluene at 25 mg/mL) were purchased from CrystalPlex (Pittsburgh, PA). Surface functionalization was performed with 5 kDa sulfhydryl-mPEG (Laysan Bio MPEG-SH-5000) using a 2 step ligand exchange method published previously.[15] First, 425 μL of choloroform and 900 μL of thioglycolic acid (Sigma T3758) were added to 130 μL of the stock QD solution. This was stirred vigorously at room temperature for 7 h. The resulting mixture was precipitated with an equal volume of acetone containing 1.85 wt % tetramethylammonium hydroxide pentahydrate (Sigma T7505). QDs were obtained by centrifugation at 1000*g* for 5 min. This was followed by three additional acetone washes. QDs were then reacted with mPEG-SH 5 kDa (QD:mPEG molar ratio of 1:11 250) in 50 mM borate buffer at 60 °C for 60 min. Excess PEG was removed through purification using 50 kDa Amicon ultracentrifuge tube. Hydrodynamic diameter of the QDs was determined by dynamic light scattering using a Malvern Nano ZS. Transmission electron microscopy was performed to image and measure core QD diameter. PEG surface modification was validated against thioglycolic acid functionalized QD (after first step) gel-electrophoresis in 0.7 wt % agarose gels at 135 V for 15 min.

Fluorescent Labeling of *Griffonia simplicifolia* Lectin 1 (GSL-1, for Blood Vessel Staining) with Alexa Fluor 647 NHS. Alexa Fluor 647 conjugated *G. simplicifolia* Lectin 1 (GSL1-A647) was prepared by adding 100 μL of 10 mg/mL unconjugated GSL-1 in 100 mM sodium bicarbonate buffer (pH 8.3) to 100 μg of lyophilized Alexa Fluor 647 NHS ester. The mixture was vortexed and incubated at room temperature overnight and purified by size exclusion through a NAP-5 column (Sigma GE17-0853-01) and further washed with PBS and concentrated using Amicon 3 kDa cutoff centrifugal filters (Millipore, UFC500324). Degree of labeling was determined by measuring absorbance at 647 and 260 nm after completing purification and concentration steps. Degree of labeling varied from batch to batch between 4 and 6 dyes per molecule.

TEM and Size Distribution. Two microliters of a 20 nM solution of QD-PEG in double distilled water was pipetted onto a plasma treated carbon-coated TEM grid (01813-F, Ted Pella) and allowed to settle onto the carbon-layer for 5 min. Remaining solution was wicked off and the grid was allowed to dry for a further 10 min at room temperature. A FEI Tecnai 20 TEM operated at 200 kV was used to acquire the images. Size distribution was determined in ImageJ by manually measuring the diameters of particles from several images.

Agarose Gel. Ten microliters of a 20 nM solution of QD-MAA and QD-PEG was loaded into the wells of a 0.7% agarose gel and run at 135 V for 20 min. Gel was imaged using a Typhoon fluorescence scanner.

Dynamic Light Scattering Measurement. QD-MAA and QD-PEG were suspended in double distilled water at a concentration of 5 nM, and peak intensity in the number distribution was measured for each particle.

Characterization and Quantification of Protein Corona. *Preparation of Gold Nanoparticles.* The 50 and 100 nm gold nanoparticles were prepared using methods published previously.[14,23] First, 15 nm gold nanoparticles were prepared by citrate reduction method. Briefly, 100 mL of 0.25 mM chloroauric acid (Sigma) was boiled with vigorous stirring. To this solution was added 1 mL of 3.3% aqueous sodium citrate dibasic trihydrate (Sigma). The mixture was boiled for a further 10 min, and it appearance changed from clear to dark purple to bright red at the end. The solution was brought to room temperature by cooling in an ice bath. Size and concentration were measured using DLS and UV absorbance spectroscopy as published previously. The 50 and 100 nm gold nanoparticles were prepared from these 15 nm seeds using seed mediated growth. Briefly, 967 μL (for 50 nm) or 997 μL (for 100 nm) of 25 mM chloroauric acid (Sigma) was added to flasks containing 93.75 or 96.7 mL of water, respectively, with vigorous stirring. To these mixtures, 967 μL (for 50 nm) or 997 μL (for 100 nm) of 15 mM sodium citrate tribasic dehydrate was added followed by 3.35 mL (for 50 nm) or 0.305 mL (for 100 nm) of 2.4 nM 15 nm gold nanoparticles seeds prepared in the first step. Finally, 967 μL (for 50 nm) or 997 μL (for 100 nm) of 25 mM hydroquinone (Sigma) was added to respective mixtures to reduce and grow under stirring overnight. The mixtures were stabilized with Tween (final concentration 0.05% Tween 20) and concentrated by centrifugation using 50 mL Falcon tubes (1800*g* for 2 h for 50 nm and 1000*g* for 100 nm for 2 h). Concentrated stocks were stored 4 °C in the dark until surface modification.

Preparation of PEGylated Gold Nanoparticles. Surface modification of prepared gold nanoparticles with PEG was done as described previously.[14,23] Briefly, 5 kDa methoxy-PEG-SH (Laysan Bio) was dissolved in water at 5 PEG/nm^2 of nanoparticle surface area. This was added to the corresponding amount of gold nanoparticles in an 1.5 mL Eppendorf tube and vortexed. The mixture was heated at 60 °C for 1 h to

DOI: 10.1021/acsnano.6b01879
ACS Nano 2016, 10, 5468–5478

complete the reaction. Excess PEG was removed through subsequent centrifugation (1800*g* for 35 min at 4 °C) and supernatant removal. The pellet was washed and centrifuged 3 times with 1× PBS. The surface modified PEGylated gold nanoparticles were stored 4 °C in the dark until injection.

Preparation of PEGylated Silica Nanoparticles. The 50 and 100 nm amine functionalized silica nanoparticles were purchased from nanoComposix (Catalog nos.: SIAN50-10M and SIAN100-10M). The buffer of these nanoparticles was exchanged with HEPES (0.1 M, pH = 8.5) through 2 washes with centrifugation (17 000*g* for 50 nm particles and 3000*g* for 100 nm particles for 30 min). Similar to gold nanoparticles, PEGylation was done at 5 PEG/nm^2 to achieve sufficient density for serum stability. The 5 kDa SVA-PEG-Maleimide was dissolved in HEPES buffer and mixed with the corresponding amount of aminated silica nanoparticles. The reaction was done for 4 h at 37 °C. This was followed by incubation with Sulfo Cy5-NHS (Lumiprobe) dissolved in HEPES at 0.25/nm^2 for 4 h at 37 °C. Excess PEG and dye were removed by washing twice with PBS and centrifugation (17 000*g* for 50 nm particles and 3000*g* for 100 nm particles for 30 min) with 1× PBS. These PEGylated silica nanoparticles were stored at 4°C in the dark until injection.

Protein Corona Characterization and Quantification. Formation, quantification, and characterization of protein corona was performed using methodology published by Walkey *et al.*[14,23] Particle sizes of 200 cm^2 of each of the 5 nanoparticle types (QD-PEG, 50 and 100 nm PEGylated gold and silica nanoparticles) were incubated with 10% mouse serum (Sigma) for 1 h at 37 °C. Incubated particles were centrifuged (QD-PEG ultracentrifugation at 240 000*g* for 30 min, 50 nm silica nanoparticles at 14 000*g* and 100 nm silica nanoparticles at 3000*g* for 30 min, and 50 nm gold nanoparticles at 1800*g* and 100 nm gold nanoparticles at 1100*g* for 30 min) to remove excess serum. The pellets were washed with PBST (1× PBS with 0.05% w/v Tween 20) and centrifuged again. This was done twice followed by another wash with 1× PBS. The pellets were transferred into new 1.5 mL Eppendorf tubes. For each sample, protein corona was stripped off the surface through reduction with 4 μL of 500 mM dithiothreitol (DTT, Bioshop) and 8 μL of 4× LDS buffer (Invitrogen) at 70 °C for 1 h. Samples were centrifuged at 18 000*g* for 15 min at room temperature. Supernatants, containing proteins, were isolated and split into two halves for running PAGE and BCA assay, which were performed as described previously,[14,23] without any modification.

Quantum Dot and GSL1-A647 Administration in Animals. Eight-week old CD-1 Nude athymic mice (Charles River Laboratories, Canada) were used for animal studies. Briefly, 150 μL of the QD-PEG solution (1× sterile PBS; Dosing: 400 pmol/animal [7.6 mg/kg for typical 25 g mouse] for retention quantification and 4000 pmol/animal [76 mg/kg for typical 25 g mouse] for whole organ imaging) was injected intravenously *via* the tail vein and allowed to accumulate in different tissues over 72 h in order to allow for cell uptake to occur. For imaging mouse vasculature, 0.150 mg of GSL1-A647 (1 mg/mL) was injected *via* tail vein 5 min prior to perfusion. For imaging tumor tissues, an orthotopic breast cancer model was developed by injecting 5 × 10^6 MDA-MB-231 cells expressing tdTomato (donated generously by Dr. Kathleen Kelly, NCI, Bethesda, MD) under the mammary fat pad. Cell injections were done in 50:50 1×PBS/Matrigel solution. Tumor was allowed to grow for 8−10 weeks. The animal protocol was approved by University of Toronto.

Transcardial Perfusion Fixation. Mice were anesthetized using a continuous flow of 3% isoflurane in oxygen. Transcardial perfusion fixation was performed using 60 mL of 1× PBS with Heparin (10 U/mL, Bioshop) and sodium nitrite (0.5%, Sigma-Aldrich) followed by 60 mL of monomer solution containing 4% formaldehyde (Sigma-Aldrich), 1× PBS, 0.25% initiator (VA-044 azoinitiator, Wako Chemicals) and either 2%, 4% or 8% acrylamide (as specified in text). All brains were bisected sagitally in order to obtain a larger number of samples. Liver lobes were separated to obtain 2 large intact lobes for clearing.

Polymerization of Hydrogel. Harvested organs were incubated in 2%, 4%, or 8% acrylamide (matching acrylamide concentration used for perfusion) at 4 °C for 7 days with shaking. Then, supernatant was replaced with fresh monomer solution. The organ samples were placed in 50 mL Corning tubes with two small holes in the cap (made using a 1/16 in. drill). Samples were degassed in these tubes by placing them in a desiccator and applying vacuum for 2 min followed by purging with argon three times. Afterward, parafilm was quickly applied to the holes on the caps to seal the argon and prevent solution leakage. Samples were then placed in a 37 °C incubator for 3 h with shaking to polymerize the acrylamide gel. The viscous solution was poured out and the remaining solution was wicked off. Afterward, all samples were placed in 10 mL of borate buffer (200 mM sodium borate, pH 8.5, 0.1% Triton-X100 and 0.01% sodium azide) at 4 °C for storage until further use.

Clearing. Samples were wrapped in mesh bags and secured with zip ties (McMaster-Carr). Barrels were placed inside a clearing chamber, which was then connected to the board in a vertical position using Luer lock couplings for flow and Molex connectors for current (see Figure 2). Clearing at 37 °C was performed at 25 V with solution temperature of 33 °C. Due to joule heating from applied current, we estimate that this temperature corresponds to ∼37 °C inside the tissue. A circulator with a volume of 13 L (total volume of the setup including filters is 15.5 L) was used. Solution was changed when solution reached pH 8 (approximately every 2−3 days for 12 chambers). Refrigeration was required to maintain constant temperature as typical current for 12 chambers was 8 A resulting in 200 W of heat generation from electrophoresis. Flow rate was maintained between 0.5 and 1 L/min for each chamber by adding secondary pumps. The architecture of the high-throughput device allows for isolation of each cluster preventing any contamination. Each cluster can be connected to a dedicated pump, temperature regulator, and voltage with customized clearing solution. For experiments pertaining to clearing at higher temperature, clearing was performed at 25 V and 45 °C. Polarity was reversed every 2−3 days to remove black deposits on electrodes and extend their life. First, tissues were removed and stored in clearing solution; then, polarity was switched and system was allowed to run for 2 h. After 2 h, solution was removed and the system was rinsed 3 times with deionized water to wash out fine platinum particulates. Due to a dead volume of 2.5 L, the solution in the circulator was replaced with appropriate concentration in order to achieve a final concentration of 4% or 8% SDS as necessary (*e.g.*, added 4.8% to achieve 4%). Samples were then returned to their chambers and electrophoresis was restarted at the new polarity.

Whole Animal Clearing. The whole animal clearing was performed according to a procedure reported by Yang *et al.*[17] After fixation using 4% formaldehyde (Sigma-Aldrich) in 1× PBS and tissue cross-linking using 4% acrylamide in 1× PBS and 1× PBS containing 0.25% initiator (VA-044 azoinitiator, Wako Chemicals), the mouse was transcardially perfused with boric acid buffer (pH 8.5; 0.2 M) containing 8% SDS at ∼40 °C for 2 weeks (flow rate ∼1 mL/min).

End Point Processing. After 28 days of clearing or after achieving normalized optical density (OD) of <0.33, tissues were removed from clearing solution and placed in borate buffer (0.2 M sodium borate, pH = 8.5). These were incubated at 37 °C with shaking for 2 days (daily solution change) to remove SDS from cleared tissues. Next, tissues were dried and weighed to determine swelling during the clearing process. Index matching for organs was achieved by adding 3 mL of RIMS solution (88% Iohexol, 2.5% 1,4-diazabicyclo[2.2.2]octane, 50 mM sodium borate, pH 8.5, 0.01% sodium azide) to each brain, kidney, and tumor sample and 5 mL of RIMS to each liver and muscle sample due to their larger size. Samples were incubated with RIMS at 37 °C with shaking for 1 day before OD measurement.

Optical Density (OD) Measurement during Clearing. Tissues were dried and placed in 6-well plates (NEST Biotech Company Ltd.). Next, these plates were scanned using a Tecan Infinite 200 PRO plate reader at wavelengths of 488 and 647 nm. A total of 177 OD measurements were collected in each well forming a grid as shown in Figure S3a (15 × 15 circle filled). Tissue area was defined using a custom tracing algorithm ("bwboundaries" function in MATLAB followed by revisions to improve tissue area recognition) and OD was calculated by taking the mean of the measurements in this region. The relevant MATLAB code is provided in Supporting Information Code S10. OD of the tissue was determined as the average OD inside tissue boundary.

DOI: 10.1021/acsnano.6b01879
ACS Nano 2016, 10, 5468−5478

Tissue Sampling and Staining. Cleared tissues were stained with DAPI (Sigma-Aldrich, ex/em 364/454 nm) or SYTOX Green (Life Technologies, ex/em 504/523 nm) at 10 μM solutions of dye (100 pmol of dye/mg of cleared tissue) in borate buffer (200 mM sodium borate, pH 8.5, 0.1% Triton-X100 and 0.01% sodium azide). Tissues were stained for 4 days at 37 °C with shaking, rinsed with 1 mL of borate buffer for 1 day at 37 °C, and then immersed in 67% aqueous solution of 2,2′-thiodiethanol (TDE) solution before imaging.

3D Tissue Imaging. Whole organ distribution of QD-PEG was acquired by using Zeiss Lightsheet Z.1 Microscope (Clr Plan-Neofluor Objective: 20×, NA = 1.0, refractive index = 1.45). Images and movies were prepared using Bitplane Imaris.

Image Analysis. Segmentation and distance transformation was performed in Bitplane Imaris. Nuclei segmentation was achieved by first smoothing the image with a filter size of 2 μm followed by a manually guided region growing algorithm to ensure nuclei were accurately segmented. Watershed on the segmented nuclei image was used to label each nuclei with a unique identifier. Blood vessels were segmented using a manually selected local threshold after smoothing with a filter size of 2 μm. QDs were segmented without smoothing using a global threshold to avoid contaminating the data. 3D Euclidean distance transformation was performed both inside and outside the segmented vessels, and the two images were imported into Matlab along with the segmented image of nuclei and the raw and segmented images of QDs. Matlab code provided in S11 was then used to combine the positive and negative vessel distance transformation images to create a signed distance transform for vessels. Nuclei and QD fluorescence histograms were then generated by comparing nuclei centroids and QD fluorescence intensities with the signed distance transformations. Raw QD fluorescence intensity was used for the analysis although only in regions identified as positive for QDs using an automated global threshold to exclude low level background signal from the analysis.

ICP-MS for Quantitative Biodistribution and Quantum Dot Retention. Whole organs (heart, lung, brain, kidney) and sections (liver, intestine, skin, spleen) of different organs were weighed post-perfusion for subsequent quantification of biodistribution and retention of quantum dots post clearing. The organs were either frozen or underwent clearing as per experimental necessity. For organ digestion, 2 mL of nitric acid was added to finely chopped organs. Digestion was performed overnight at 70 °C in a water bath. Solutions were diluted with water and filtered with Millipore 0.22 μm PES filters (Millex GV) to remove debris to final acid concentration of 2%, matching the inline solutions on the ICP-MS system. Standard curve and injected dose samples were also prepared for measurement. Cadmium content was measured using PerkinElmer NexION ICP-MS System, which is equipped with inline iridium as internal standard.

Protein Loss Quantification. Protein loss was measured using the bicinchoninic acid assay (Micro BCA Protein Quantification Kit, Pierce Biotechnology). Briefly, 50 μL of supernatant from passively cleared tissues was collected each day for the first week. These supernatants were combined and the solution was precipitated overnight at 4 °C using 100 μL of 72% (w/v) trichloroacetic acid (Sigma-Aldrich). This was centrifuged at 18 000*g* for 15 min to obtain a pellet. The pellet was suspended in 950 μL of acetone and precipitated overnight at −80 °C. This was again centrifuged at 18 000*g* for 15 min to obtain a pellet. The supernatant was removed, and precipitated protein was dissolved in 50 μL of 1× PBS. For each 50 μL sample or standard, 50 μL of the BCA solution (1.25:1:0.05 of Reagent A/B/C) was added. The reaction was conducted at 60 °C for 1 h on a thermocycler for accurate time and temperature control. Absorbance of samples and standards was measured at 562 nm using a spectrophotometer (TECAN Sunrise). Protein quantification for each tissue type was performed against BSA standards using linear regression.

ASSOCIATED CONTENT

Supporting Information

The Supporting Information is available free of charge on the ACS Publications website at DOI: 10.1021/acsnano.6b01879.

Video S1, 3D distribution of quantum dots in mouse livers (AVI)
Video S2, 3D distribution of quantum dots in mouse livers (AVI)
Video S3, 3D distribution of quantum dots in mouse kidneys (AVI)
Video S4, 3D distribution of quantum dots in mouse kidneys (AVI)
Video S5, 3D distribution of quantum dots in mouse spleen (AVI)
Video S6, probing fluorescence and tissue integrity in whole tumors (AVI)
Video S7, slice-by-slice view of whole tumor showing organization of tumor cells and vasculature (AVI)
Video S8, light sheet microscopy of whole tumor vasculature (AVI)
Video S19, slice-by-slice view of whole tumor showing organization of tumor vasculature post light sheet microscopy (AVI)
Code S10, Instructions(TXT)
Code S10, Matlab script used for calculating OD for an organ (TXT)
Code S11, Matlab scripts used to map nuclei and QDs against distance from vessels (TXT)
Characterization of quantum dots (Figure S1); *in vivo* retention of nanoparticles with different sizes (Figure S2); parametric characterization of clearing rate in different organs (Figure S3); increasing SDS concentration from 4% to 8% does not affect rate of clearing (Figure S4); QD-PEG imaged and analyzed in multiple organs (Figure S5) (PDF)

AUTHOR INFORMATION

Corresponding Author

*E-mail: warren.chan@utoronto.ca.

Author Contributions

¶S.S. and A.M.S. contributed equally to this work.

Notes

The authors declare no competing financial interest.

ACKNOWLEDGMENTS

We would like to acknowledge the Canadian Institutes of Health Research (CIHR) and Natural Sciences and Engineering Research Council (NSERC) for supporting the project. S, S. acknowledges CIHR and A. M. S., D. G., and Y. Y. C. acknowledge NSERC for student fellowships.

REFERENCES

(1) Nichols, J. W.; Bae, Y. H. Odyssey of a Cancer Nanoparticle: From Injection Site to Site of Action. *Nano Today* **2012**, *7*, 606−618.
(2) Chauhan, V. P.; Stylianopoulos, T.; Boucher, Y.; Jain, R. K. Delivery of Molecular and Nanoscale Medicine to Tumors: Transport Barriers and Strategies. *Annu. Rev. Chem. Biomol. Eng.* **2011**, *2*, 281−298.
(3) Park, K. Facing the Truth about Nanotechnology in Drug Delivery. *ACS Nano* **2013**, *7*, 7442−7447.
(4) Walkey, C. D.; Chan, W. C. W. Understanding and Controlling the Interaction of Nanomaterials with Proteins in a Physiological Environment. *Chem. Soc. Rev.* **2012**, *41*, 2780−2799.
(5) Chauhan, V. P.; Jain, R. K. Strategies for Advancing Cancer Nanomedicine. *Nat. Mater.* **2013**, *12*, 958−962.
(6) Weissleder, R. Scaling Down Imaging: Molecular Mapping of Cancer in Mice. *Nature Rev. Cancer* **2002**, *2*, 11−18.

DOI: 10.1021/acsnano.6b01879
ACS Nano 2016, 10, 5468−5478

(7) Ntziachristos, V.; Ripoll, J.; Wang, L. V.; Weissleder, R. Looking and Listening to Light: the Evolution of Whole-Body Photonic Imaging. *Nat. Biotechnol.* **2005**, *23*, 313−320.
(8) Ntziachristos, V. Going Deeper than Microscopy: the Optical Imaging Frontier in Biology. *Nat. Methods* **2010**, *7*, 603−614.
(9) Chung, K.; Wallace, J.; Kim, S.-Y.; Kalyanasundaram, S.; Andalman, A. S.; Davidson, T. J.; Mirzabekov, J. J.; Zalocusky, K. A.; Mattis, J.; Denisin, A. K.; Pak, S.; Bernstein, H.; Ramakrishnan, C.; Grosenick, L.; Gradinaru, V.; Deisseroth, K. Structural and Molecular Interrogation of Intact Biological Systems. *Nature* **2013**, *497*, 332−337.
(10) Tomer, R.; Ye, L.; Hsueh, B.; Deisseroth, K. Advanced CLARITY for Rapid and High-Resolution Imaging of Intact Tissues. *Nat. Protoc.* **2014**, *9*, 1682−1697.
(11) Kim, S.-Y.; Chung, K.; Deisseroth, K. Light Microscopy Mapping of Connections in the Intact Brain. *Trends Cognit. Sci.* **2013**, *17*, 596−599.
(12) Kim, B. Y. S.; Rutka, J. T.; Chan, W. C. W. Nanomedicine. *N. Engl. J. Med.* **2010**, *363*, 2434−2443.
(13) Lundqvist, M.; Stigler, J.; Elia, G.; Lynch, I.; Cedervall, T.; Dawson, K. A. Nanoparticle Size and Surface Properties Determine the Protein Corona with Possible Implications for Biological Impacts. *Proc. Natl. Acad. Sci. U. S. A.* **2008**, *105*, 14265−14270.
(14) Walkey, C. D.; Olsen, J. B.; Guo, H.; Emili, A.; Chan, W. C. W. Nanoparticle Size and Surface Chemistry Determine Serum Protein Adsorption and Macrophage Uptake. *J. Am. Chem. Soc.* **2012**, *134*, 2139−2147.
(15) Sykes, E. A.; Dai, Q.; Tsoi, K. M.; Hwang, D. M.; Chan, W. C. W. Nanoparticle Exposure in Animals can be Visualized in the Skin and Analysed *via* Skin Biopsy. *Nat. Commun.* **2014**, *5*, 3796.
(16) Yang, B.; Treweek, J. B.; Kulkarni, R. P.; Deverman, B. E.; Chen, C. K.; Lubeck, E.; Shah, S.; Cai, L.; Gradinaru, V. Single-Cell phenotyping within Transparent Intact Tissue through Whole-Body Clearing. *Cell* **2014**, *158*, 945−958.
(17) Liang, X.; Grice, J. E.; Zhu, Y.; Liu, D.; Sanchez, W. Y.; Li, Z.; Crawford, D. H. G.; Le Couteur, D. G.; Cogger, V. C.; Liu, X.; Xu, Z. P.; Roberts, M. S. Intravital Multiphoton Imaging of the Selective Uptake of Water-Dispersible Quantum Dots into Sinusoidal Liver Cells. *Small* **2015**, *11*, 1711−1720.
(18) Åkerman, M. E.; Chan, W. C.; Laakkonen, P.; Bhatia, S. N.; Ruoslahti, E. Nanocrystal Targeting *in vivo*. *Proc. Natl. Acad. Sci. U. S. A.* **2002**, *99*, 12617−12621.
(19) Pollinger, K.; Hennig, R.; Bauer, S.; Breunig, M.; Tessmar, J.; Buschauer, A.; Witzgall, R.; Goepferich, A. Biodistribution of Quantum Dots in the Kidney after Intravenous Injection. *J. Nanosci. Nanotechnol.* **2014**, *14*, 3313−3319.
(20) Yu, M.; Zheng, J. Clearance Pathways and Tumor Targeting of Imaging Nanoparticles. *ACS Nano* **2015**, *9*, 6655−6674.
(21) Choi, H. S.; Liu, W.; Misra, P.; Tanaka, E.; Zimmer, J. P.; Ipe, B. I.; Bawendi, M. G.; Frangioni, J. V. Renal Clearance of Quantum Dots. *Nat. Biotechnol.* **2007**, *25*, 1165−1170.
(22) Choi, C. H. J.; Zuckerman, J. E.; Webster, P.; Davis, M. E. Targeting Kidney Mesangium by Nanoparticles of Defined Size. *Proc. Natl. Acad. Sci. U. S. A.* **2011**, *108*, 6656−6661.
(23) Walkey, C. D.; Olsen, J. B.; Song, F.; Liu, R.; Guo, H.; Olsen, D. W.; Cohen, Y.; Emili, A.; Chan, W. C. Protein Corona Fingerprinting Predicts the Cellular Interaction of Gold and Silver Nanoparticles. *ACS Nano* **2014**, *8*, 2439−2455.

DOI: 10.1021/acsnano.6b01879
ACS Nano 2016, 10, 5468−5478